Supporting Information

Nanofabrication of Au nanoparticles over conductive metallohydrogel nanofibers for nanocatalysis application

Manish Kumar Dixit, Déborah Chery, Chinthakuntla Mahendar, Christophe Bucher and Mrigendra Dubey*

Dr. Mrigendra Dubey, Chinthakuntla Mahendar

Soft Materials Research Laboratory, Discipline of Metallurgy Engineering and Materials Science, Indian Institute of Technology Indore, Khandwa Road, Simrol, Indore 453552, India

E-mail: mdubey@iiti.ac.in

Dr. Christophe Bucher and Dr. Déborah Chery

Univ Lyon, Ens de Lyon, CNRS UMR 5182, Université Claude Bernard Lyon 1, Laboratoire de Chimie, Lyon, France

Mr. Manish Kumar Dixit

Department of Chemistry, Indian Institute of Technology (Banaras Hindu University), Varanasi 221005, U.P., India.

Table of Contents: **Pages**

EXPERIMENTAL SECTION

Rheological Study:

The rheological measurements were performed on freshly prepared metallohydrogel with (AuCPH) and without AuNps (CPH) in triplicate. The measurements were carried out using a stress-controlled rheometer model *Anton Paar Quality Control Rheometer RheolabQC* instrument equipped with stainless steel parallel plates (20 mm diameter, 0.2 mm gap). Experiments were performed on freshly prepared metallohydrogel (1 % w/v). Linear viscoelastic regions of the metallogel samples were determined by measuring the storage modulus, G′ (associated with energy storage) and the loss modulus, G″ (associated with the loss of energy) as a function of stress amplitude (Dynamic oscillatory frequency of 10 rad s^{-1}). The following tests were performed: increasing amplitude of oscillation up to 100 % apparent strain on shear, time and frequency sweeps at 25 °C (20 min and range from 0.05 to 100 rad s^{-1}, respectively) and a heating run to 100 °C at a scan rate of 5 °C min^{-1}.

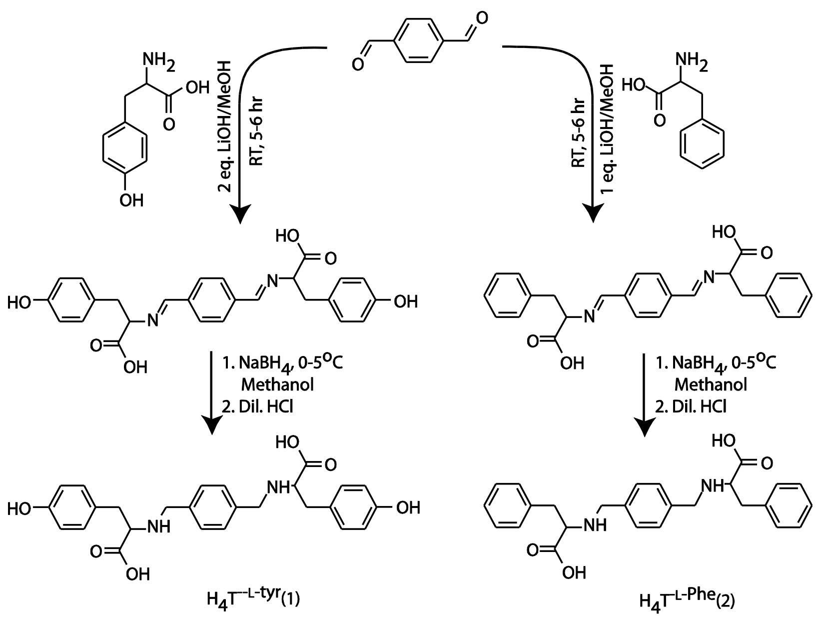

Scheme S1. Synthetic route adopted for the synthesis of **1** and **2**.

Table S1. Gelation details isomer, cation and solvent*

S.N.	Solvent	1+LiOH+Zn$(NO_3)_2$	2+LiOH+Zn$(NO_3)_2$
1.	Water	**G**	GS
2.	Acetonitrile	S	S
3.	Methanol	S	S
4.	Ethanol	S	S
5.	DMSO	S	S

*Where, G= gel, GS= gelatinous solution and S= turbid sol.

Table S2. Gel or sol formation of **1** with different alkali bases and Zn$(NO_3)_2$

Solvent	1/Li^+/Zn^{2+}	1/Na^+/Zn^{2+}	1/K^+/Zn^{2+}	1/Cs^+/Zn^{2+}
Water	G	WG	WG	S

*Where, G= gel, WG= weak gel and S= sol.

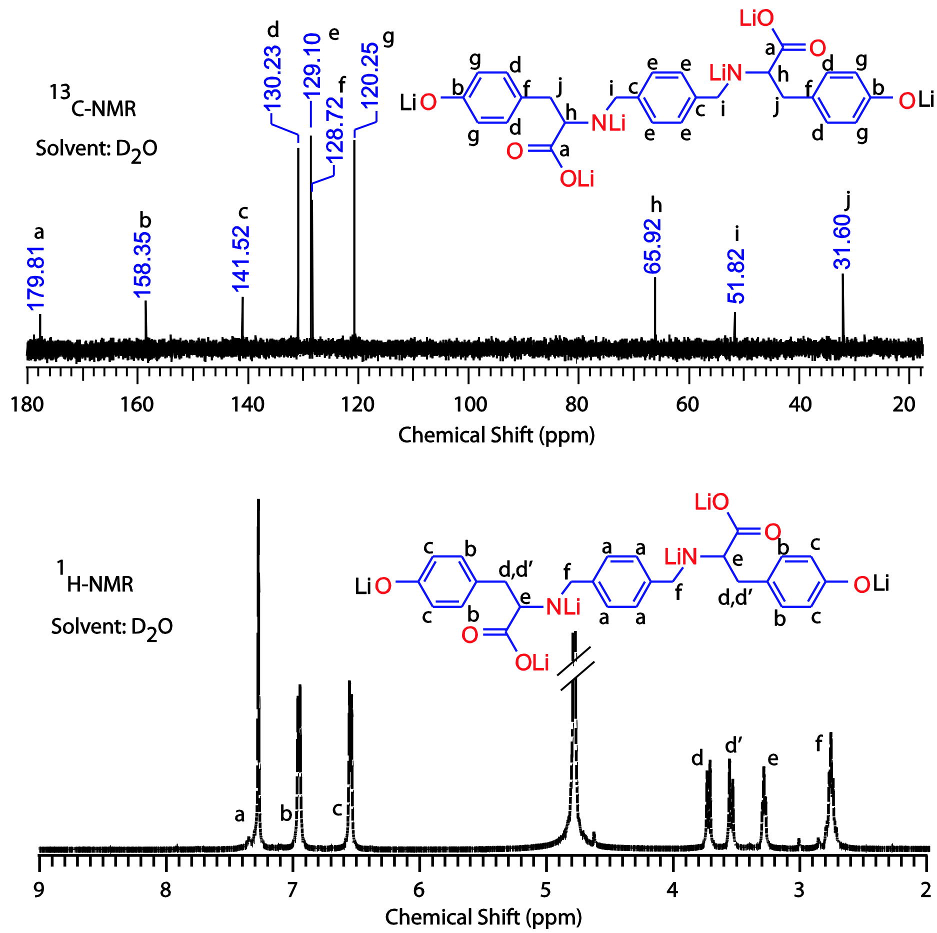

Figure S1. ^{13}C (above) and ^{1}H NMR (below) spectrum of LiOH deprotonated **1** (D_2O). Chemical structure of **1** along with alphabetic assignment of carbons and protons, respectively, and its corresponding peak is shown in spectrum.

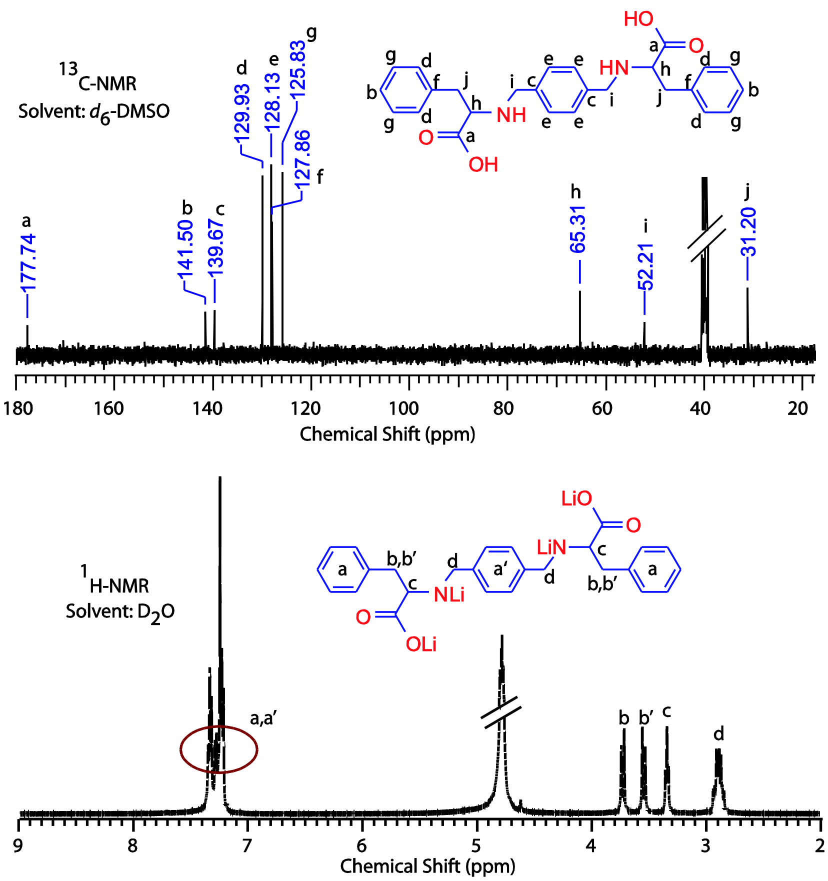

Figure S2. ^{13}C NMR (d_6-DMSO; above) spectra of **2** and ^{1}H NMR (below) spectrum of LiOH deprotonated **2** (D_2O). Chemical structure of **2** along with alphabetic assignment of carbons and protons, respectively, and its corresponding peak is shown in spectrum.

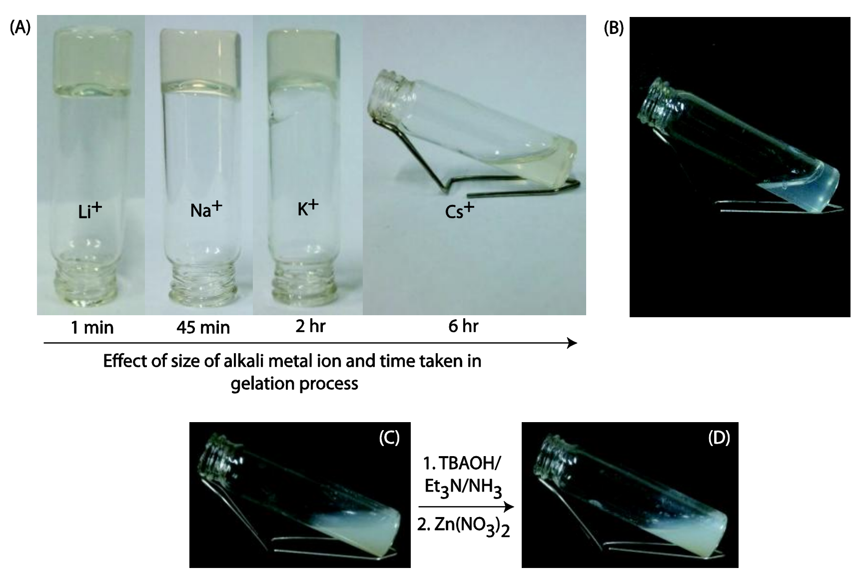

Figure S3. (A) Monitoring of gel strength and effect of size of alkali metal ions Li^+, Na^+, K^+ and Cs^+. Moving from Li^+ to Cs^+ gelation time increases and weaken the strength of gel. (B) Gelatinous solution obtained when we replace H_4T^{-L-tyr} with H_4T^{-L-Phe} under similar gel synthesis conditions, (C) and (D) Gelation test with other bases like TBAOH or Et_3N or NH_3 produce turbid solutions.

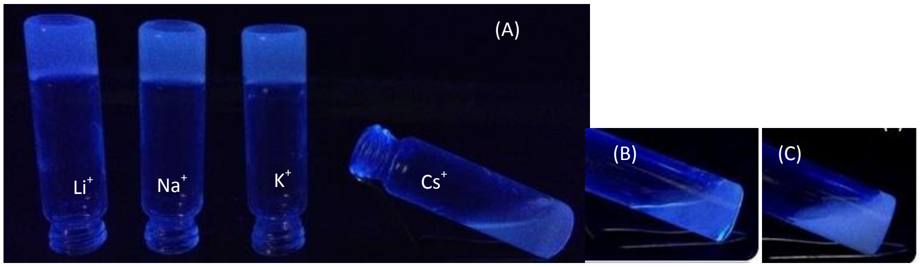

Figure S4. (A) Metallogel/solution under UV lamp (λ_{em}=365 nm), (B) H_4T^{-L-Phe} produced fluorescent gelatinous solution under similar conditions and (C) TBAOH deprotonated H_4T^{-L-tyr} produced fluorescent precipitate under similar condition to gelation.

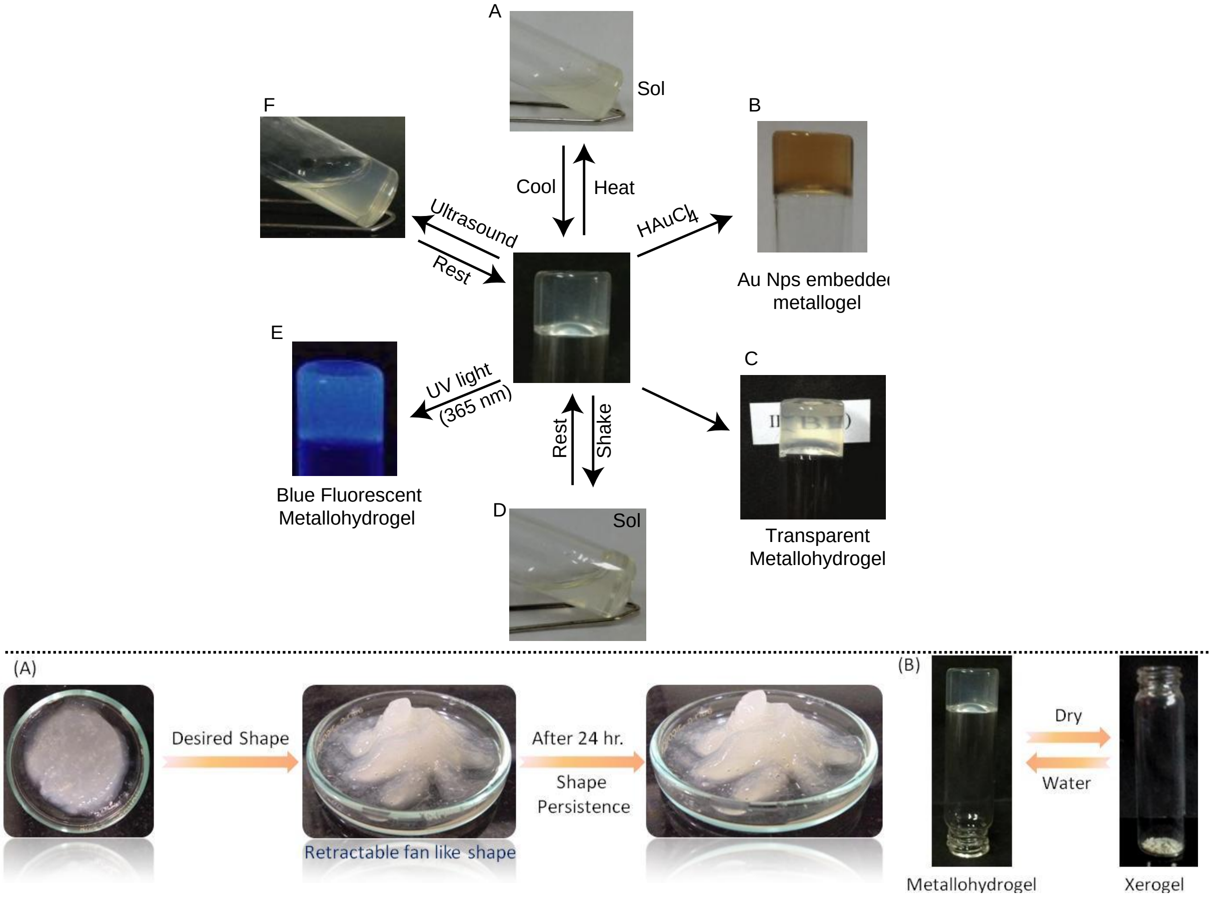

Figure S5. (Upper) Various properties of metallohydrogel- (A), (D) and (F) shows the multi-stimuli responsive behaviour of metallohydrogel towards external stimuli temperature, mechanical and ultrasound, (B) Au nanoparticle containing metallohydrogel (AuCPH), (C) The freshly prepared transparent metallogel, through which word is readable, (E) Blue fluorescent metallohydrogel under UV lamp (365 nm). (Lower) (A) Shape persistance property of metallohydrogel which was retained even after 24 hrs and (B) Reswelling behaviour shown by metallohydrogel (CPH).

Note: Thermoreversibility was monitored at 70°C.

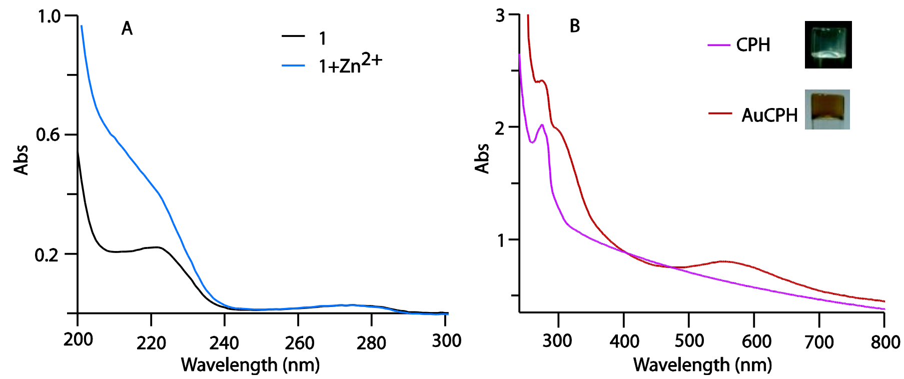

Figure S6. UV-vis spectra of **(A)** $T^{-L-tyr\ 4-}$ ($1X10^{-5}$M, H_2O, black line) and upon addition of $Zn(NO_3)_2$ in blue line and (B) A comparsion spectra of diluted AuCPH (red line) and CPH (voilet line).

Note: AuCPH shows the characteristic plasmon band at *ca.* 560 nm for AuNPs.

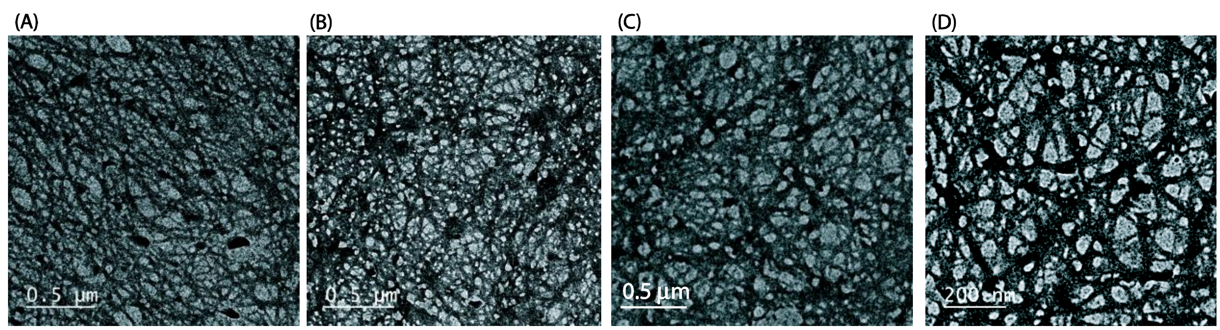

Figure S7: TEM images of diluted CPH ($1X10^{-5}$M) at two different magnification.

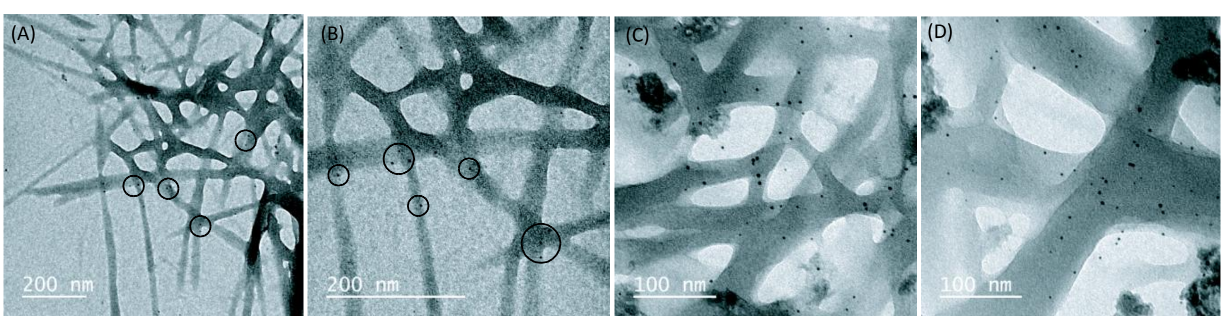

Figure S8: TEM images of diluted AuCPH captured at three different magnifications.

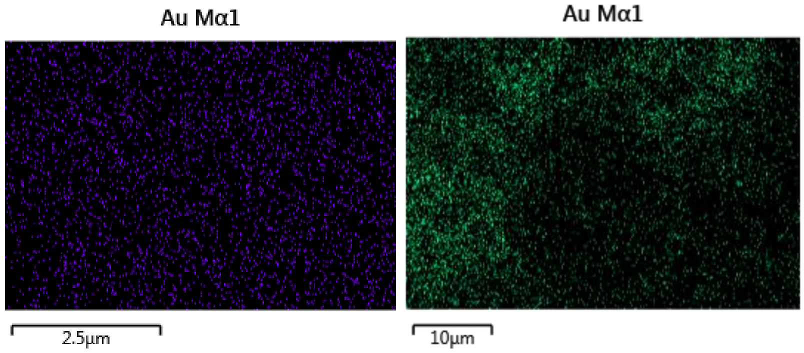

Figure S9. FE-SEM elemental maps for AuNps dispersion in xerogel state performed twice to ensure the homogeneous dispersion. The colors in the element map are violet (left) and green (right) for AuNPs.

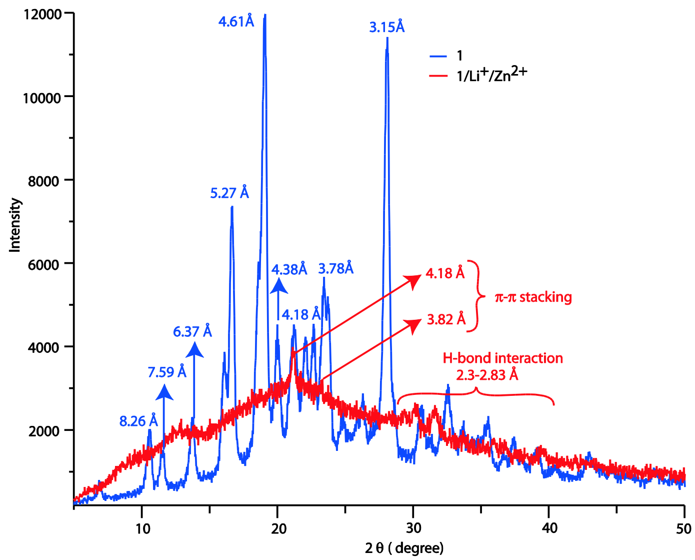

Figure S10. Powder X-Ray Diffraction pattern of **1** (blue line) and xerogel (Red line).

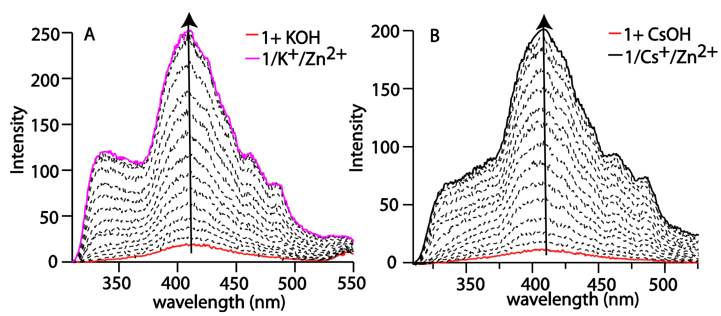

Figure S11. Fluorescence titration of (A) KOH deprotonated $T^{-L-tyr4-}$ ($1x10^{-2}$M, H_2O, λ_{ex}= 275 nm) with $Zn(NO_3)_2$ shows the gradual enhancement in intensity of the peak at 411 nm (stoke's shift= 12000 cm^{-1}) and a new peak generation at 338 nm with no noticeable shift and (B) CsOH deprotonated $T^{-L-tyr4-}$ ($1x10^{-2}$M, H_2O, λ_{ex}= 275 nm) produced the same fluorescence spectra.

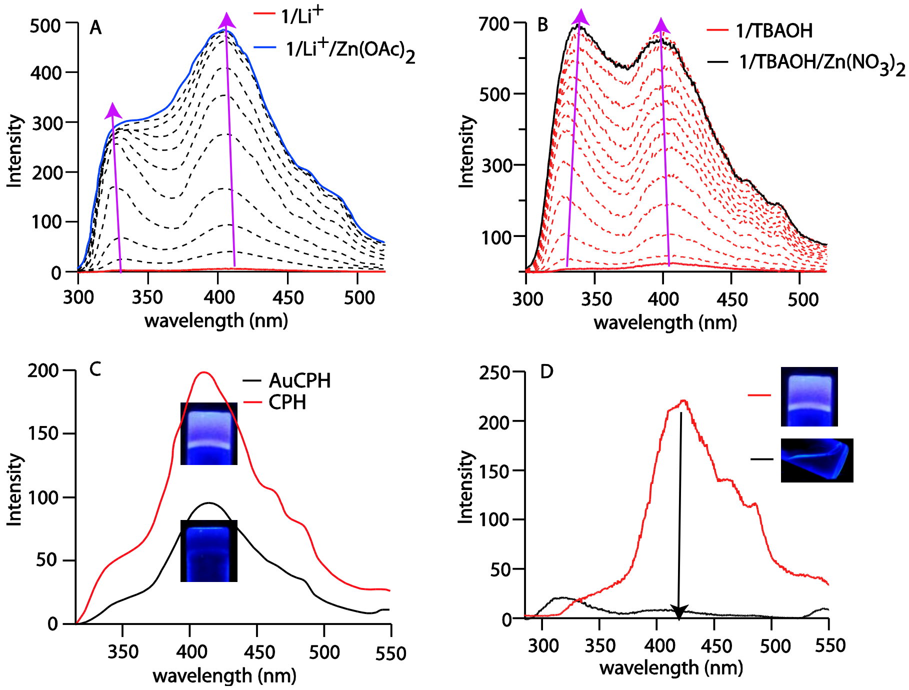

Figure S12. Fluorescence experiment **(A)** LiOH deprotonated $T^{-L-tyr4-}$ (red line) appears 330 nm and 408 nm which upon gradual addition of 1.2 equivalent of $Zn(OAc)_2$ (blue line) increases the emmision intensity, **(B)** Fluorescence spectra of TBAOH deprotonated $T^{-L-tyr4-}$ (10^{-2}M, H_2O) with $Zn(NO_3)_2$ shows enhancement in instensity with smalll red shift of 8 nm at 330 nm peak and small blue shift of 6 nm of 406 nm peak, **(C)** A comparative fluorescence spectra of CPH and AuCPH and **(D)** Fluorecence spectra of CPH upon treatment with HCl.

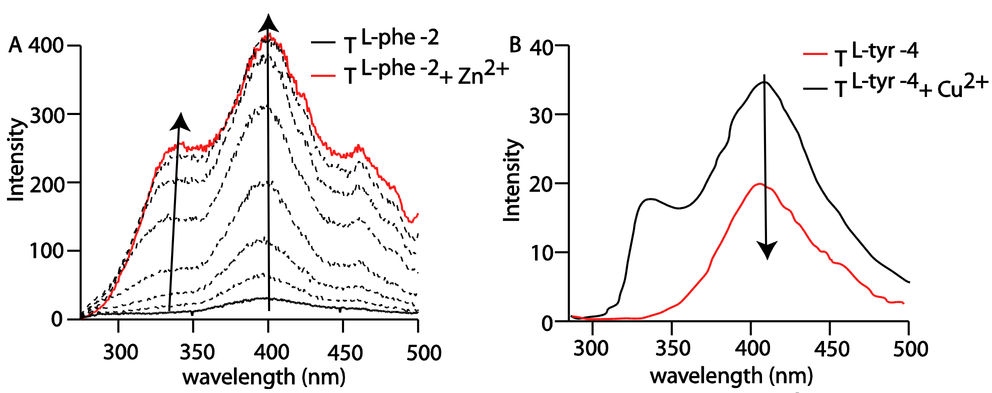

Figure S13. (A) Fluorescence spectra of LiOH deprotonated H_4T^{-L-Phe} (10^{-2}M, H_2O, λ_{ex}= 258 nm) with $Zn(NO_3)_2$ (1M, H_2O) and (**B**) Addition of $Cu(NO_3)_2$ to $T^{-L-tyr4-}$ (10^{-2}M, H_2O, LiOH deprotonated) produced nonfluorescent complex.

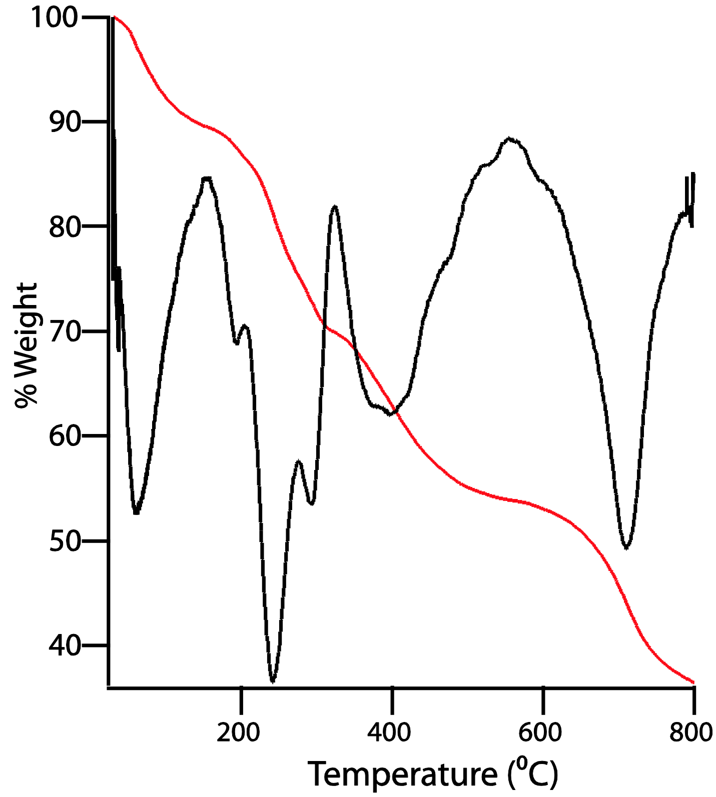

Figure S14. The Thermo Gravimetric Analysis (TGA, red line) along with derivative plot (black line) for the isolated compound from xerogel (washed with H_2O to remove extra salts and vacuum dried) shows weight loss of 10.46 % close to the molecular weight of $3H_2O$ (10.21 %). Three H_2O molecules were removed up to nearly ~180^{o}C from xerogel which was indicative towards the presence of water in strong interaction with gelator molecule.

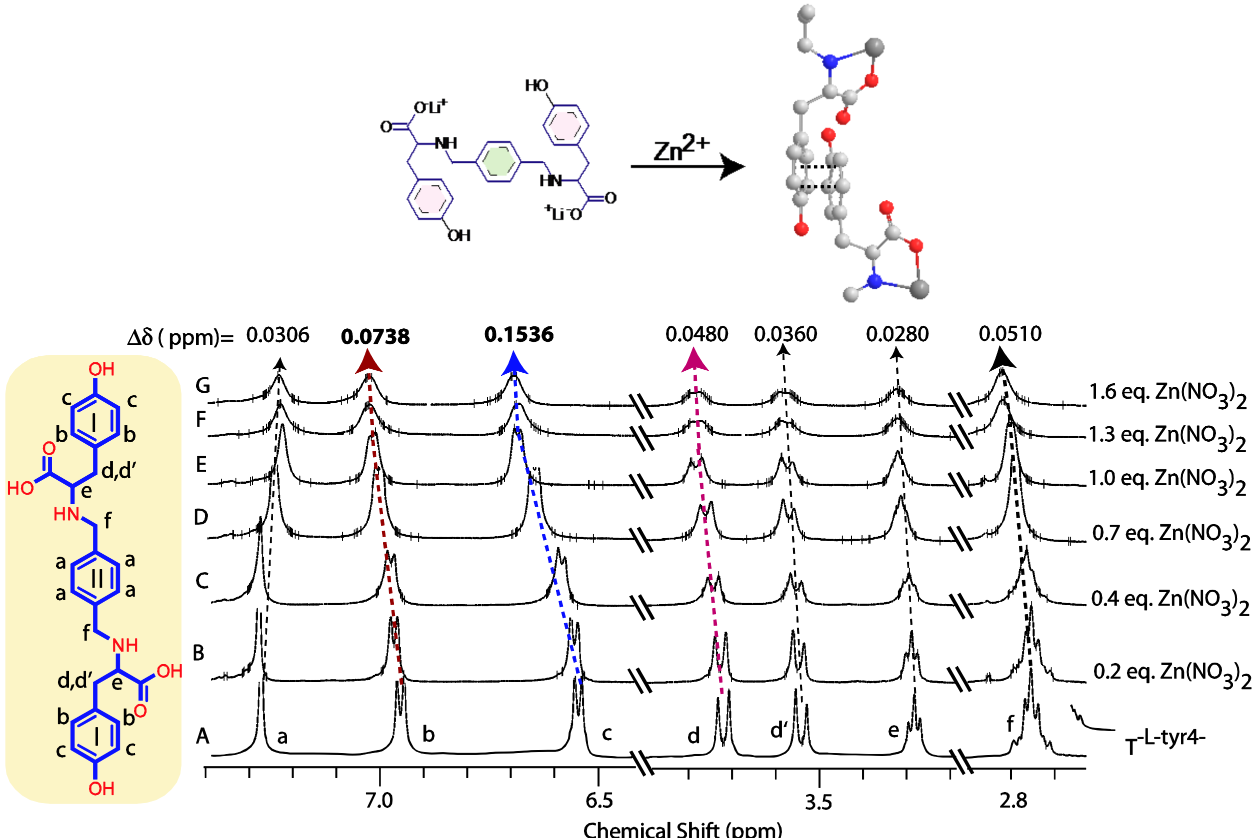

Figure S15. [1]H NMR titration of deprotonated $T^{-L-tyr4-}$ *vs.* $Zn(NO_3)_2$ in D_2O. H_4T^{-L-tyr} structure along with labelling of proton (left side). The upper structure represent the result of [1]H NMR titration as well as possibility of π-π stacking between phenolic ring protons.

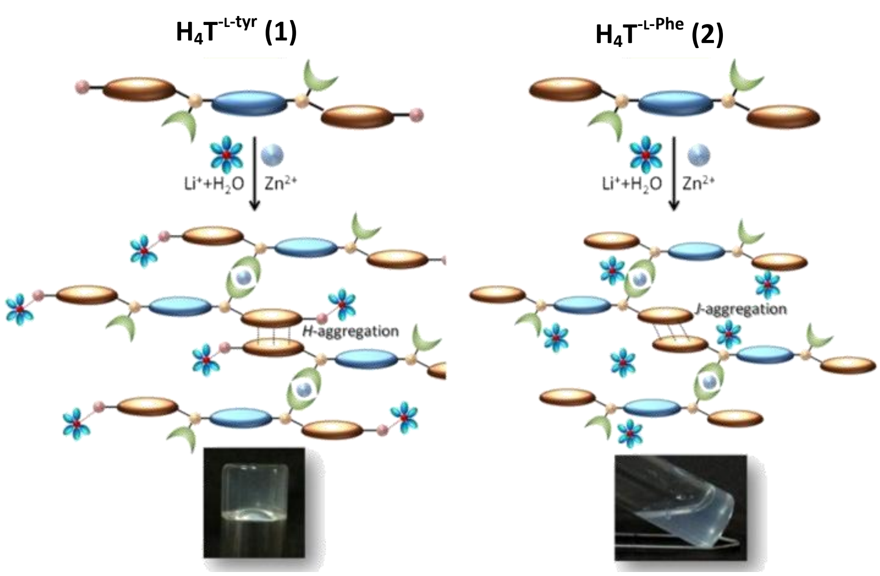

Figure S16. Model represents possibility of molecular arrangements for metallohydrogel and solution obtained from pro-ligands **1** and **2**, respectively.

Note: Gel formation fluorscence titration experiment (Figure 3B) suggests that after addition of $Zn(NO_3)_2$ to the deprotonated pro-ligand, molecules arrange themself into a higher energy state *via* blue shift of 4 nm whereas deprotonated pro-ligand **2** shows red shift upon Zn^{2+} addition indicative towards the acheivement of lower energy state *via* *J*-type aggregation.

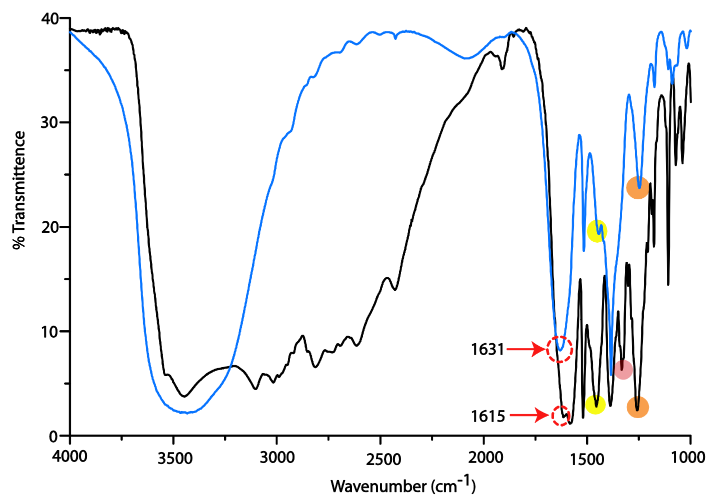

Figure S17. FTIR spectral overlap of $H_4T^{-L\text{-}tyr}$ (**1**, black line) and CPH (blue line).

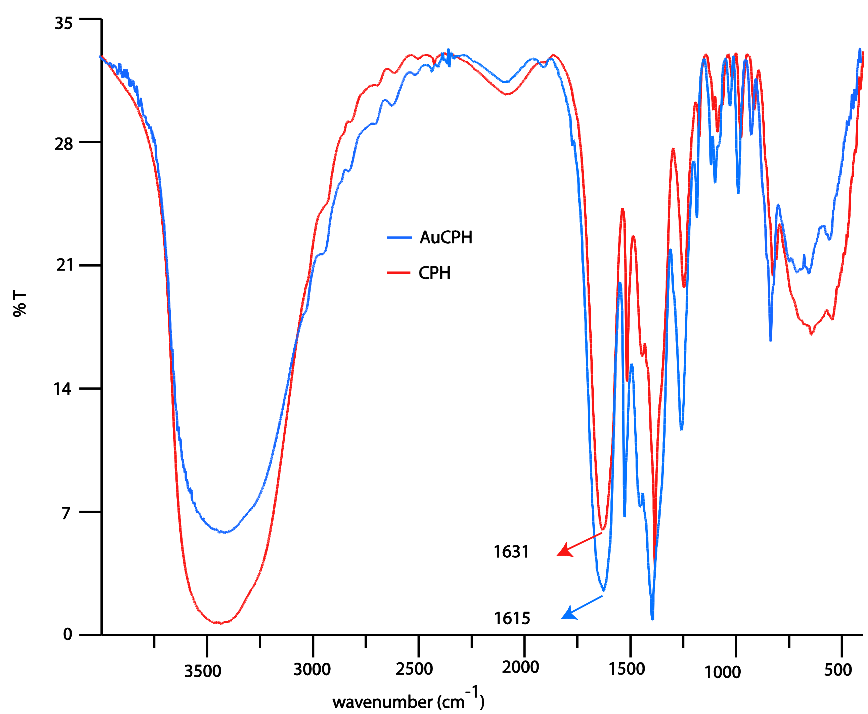

Figure S18. FTIR spectral overlap of CPH (red line) and AuCPH (blue line).

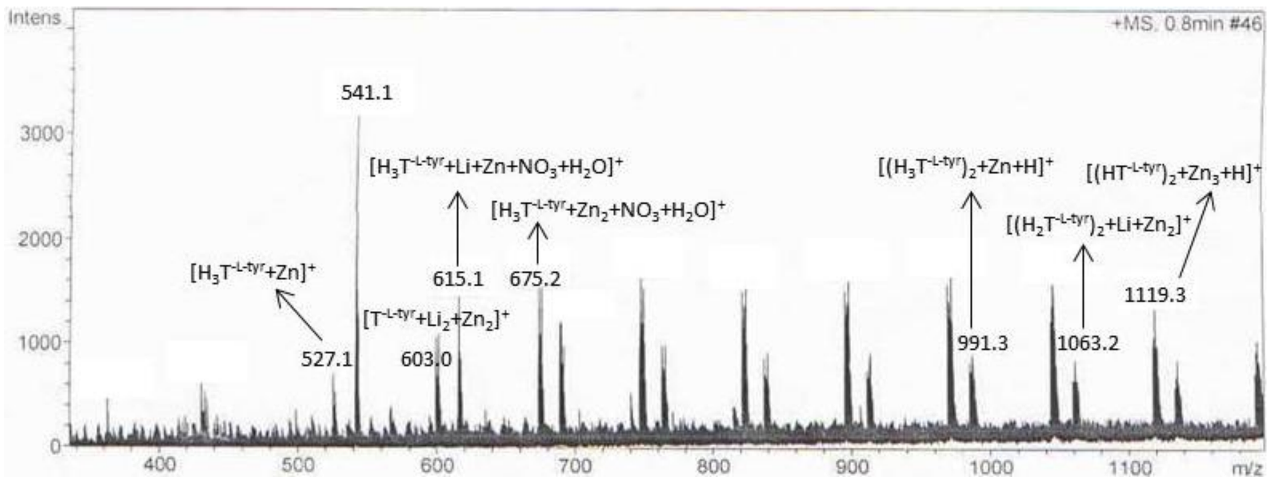

Figure S19. ESI-MS spectrum of diluted metallohydrogel (CPH) in positive mode along with labelling of molecular ion peaks.

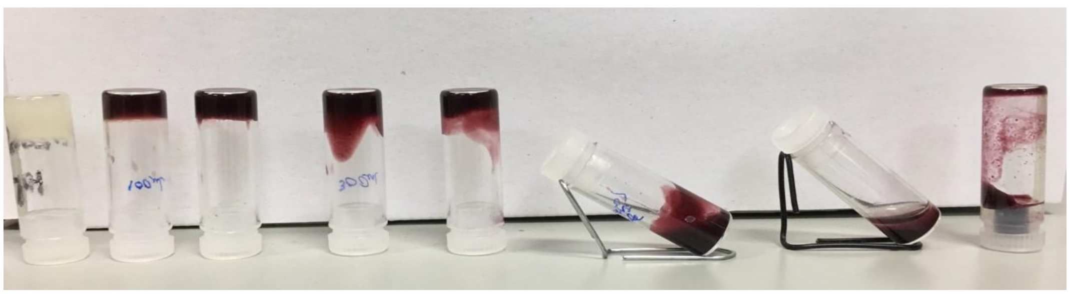

Figure S20. Effect of amount of $HAuCl_4$ solution addition to metallohydrogel weakens the gel strength.

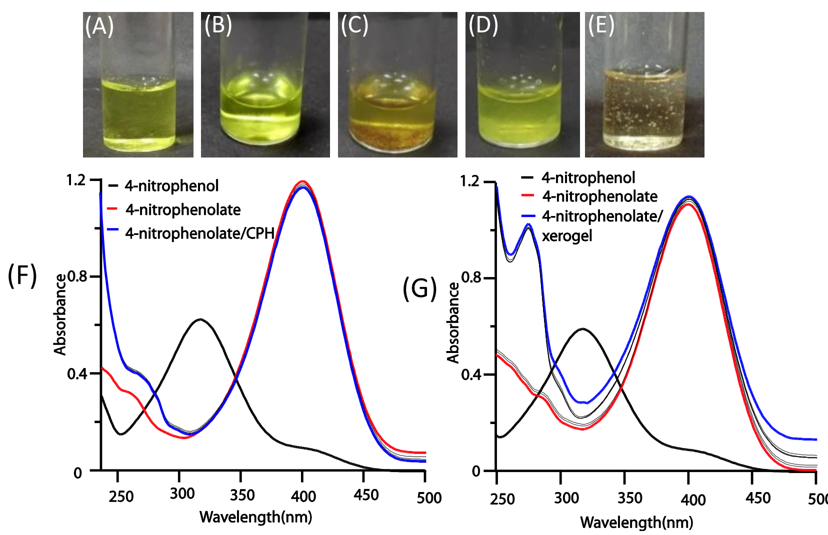

Figure S21. Pictures show (A) aqueous solution of 4-nitrophenol, the visual changes occurred upon addition of (B) $NaBH_4$ to aqueous solution of 4-nitrophenol, (C) xerogel (obtained from AuCPH) to 4-NP/$NaBH_4$ solution, (D) CPH to 4-NP/$NaBH_4$ solution, (E)

AuCPH to 4-NP/$NaBH_4$ solution. UV-vis spectra of *aq*. 4-nitrophenol upon addition of (F) CPH and (G) dried AuCPH as catalytic material in prescence of excess of $NaBH_4$ (100 equivalent of 4-nitrophenol).

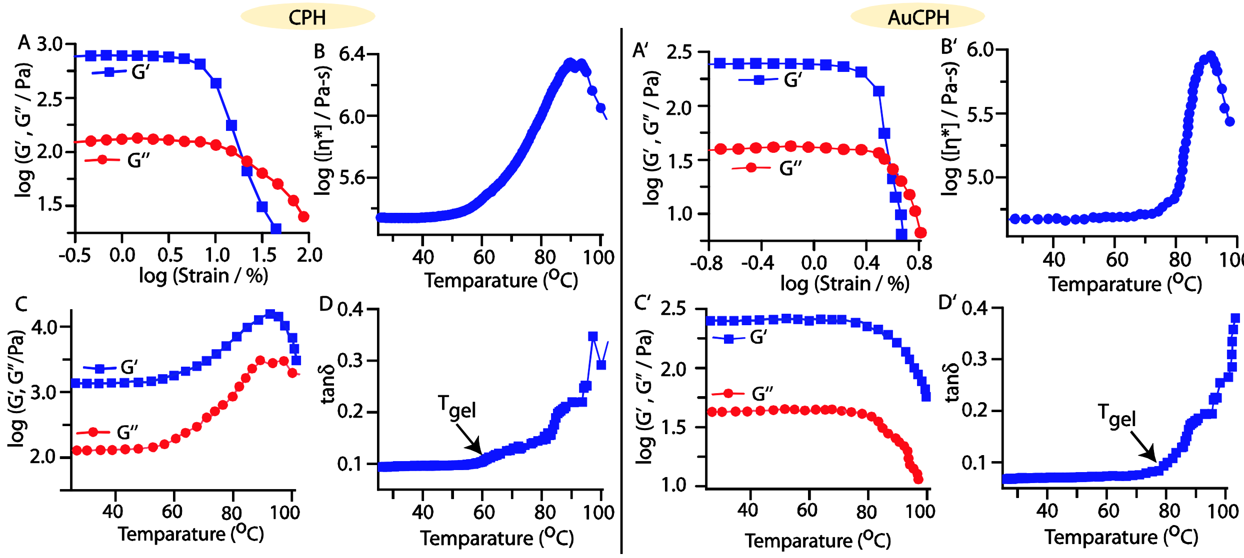

Figure S22. Rheology of CPH and AuCPH (A), (A') Dynamic strain sweep experiment at 10 rad s^{-1} and temperature 25 °C; (D), (D') Dynamic temperature ramp of complex viscosity measurement at 5 °C min^{-1}; (E), (E') Plot of G″ and G′ on dynamic temperature ramp and (F), (F') Dynamic temperature ramp of the loss tangent (tan δ = G″/G′) plot at 5 °C min^{-1}.

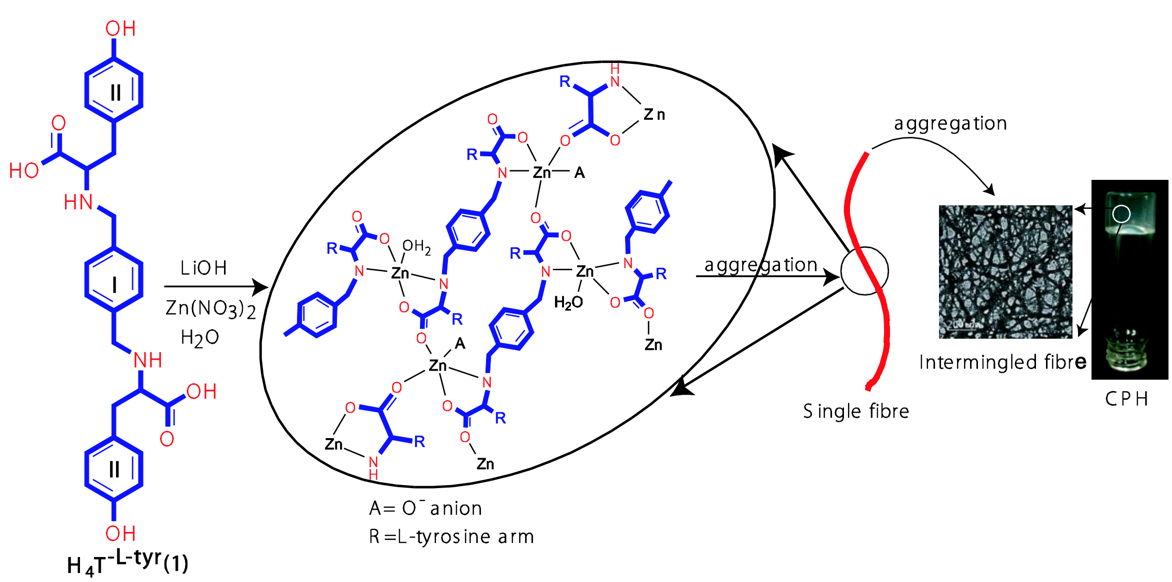

Figure S23. A schematic presentation of plausible mechanism behind metallohydrogel formation.